

Synoptic Patterns of Severe Hailstorm Events in Spain

F. de Pablo Dávila^{a*}, L.J. Rivas Soriano^a, C. Jiménez Alonso^b, M. Mora García^c
J. Riesco Martín^b

1. *Departamento de Física Fundamental, Universidad de Salamanca, Salamanca, Spain.*
2. *Agencia Estatal de Meteorología, (AEMet), Málaga, Spain*
3. *Agencia Estatal de Meteorología, (AEMet), Valladolid, Spain*

* Corresponding author address:

Dr. Fernando de Pablo
Departamento de Física Fundamental
Facultad de Ciencias. Universidad de Salamanca
Pl. de la Merced s/n
37008 Salamanca (Spain)

e-mail: fpd123@usal.es

ORCID: 0000-0003-4859-4613

26 ABSTRACT

27 A study of severe hailstorm (with size $\geq 3\text{cm}$) over Spain has been conducted
28 using 8 years (2012–2019) of data. The 73 events of heavy hail selected were classified
29 using the moisture flux at the 850 hPa pressure level (qv_{850}) and the lifted index (LI) as
30 variables and a principal component analysis, coupled with a K-means clustering, as
31 statistical technique. The application of this procedure provided four groups with their
32 respective final cluster center. We took as the salient pattern of each cluster the case
33 closest to each final cluster center. It was found that high values of low levels moisture
34 flux ($\sim 89 \text{ g m/kg s}$ on the average) are accompanied by static instability (SBCAPE \sim
35 600 J/kg and average LI ~ -4). The temperature values exceeded 20°C at the 850 hPa
36 pressure level and range between -8°C and -20°C at the 500 hPa pressure level. The
37 most typical configuration corresponded to geopotential and thermal trough at mean
38 levels of the troposphere and low pressure at low levels. Likewise, high values of
39 precipitable water ($> 35 \text{ kg/m}^2$) have been detected and the presence of storm relative
40 helicity and shear was moderate or strong in all cases.

41
42 *Keywords:* Severe hailstorms. Stability index. Cluster analysis. Spain.

1. Introduction

Hail is a meteorological phenomenon that consists of a type of precipitation made up of ice particles with a diameter equal to or greater than 5mm. Hail occurs in many areas of our planet and thus frequent severe hailstorms take place over most of Europe, causing considerable damage to buildings. This is equally the case with agricultural crops or cars, generating great economic losses. In the work of Punge and Kunz (2016) an extensive review of the characteristics of hail is carried out, with observations of Europe in recent decades. There, it is shown how, for instance, two supercells that occurred on July 27/28, 2013 activated in the vicinity of *Andreas* low pressure system caused insured damages of 2.800 million euros in Germany. Thus, it became the most costly event of insured losses during 2013 worldwide (SwissRe, 2014). A year later, hailstorms associated with the *Ela* episode that occurred between June 8-10, 2014, were responsible for insured damages of € 2.3 billion in France, Belgium and Germany. Zimmerli (2005) estimated that the potential insurance damage caused by hailstorms across Europe, with a return period of 200-300 years, may be around € 4 billion. Regarding the Iberian Peninsula, hail can be observed in any area of it and Spain is among the countries with the highest associated losses within the agriculture sector. According to Porras et al., (2013) the annual average of insurance compensation in the agricultural sector is around 240 million euros for the period 2001-2009. The hail map, based upon the damages produced in agriculture, shows the areas of maximum intensity in the Pyrenees and NE of the Iberian System (Burgaz, 2004) as well as on the east coast of the Iberian Peninsula (Saa Requejo et al., 2011).

Among the first works that identify these regions as the Spanish areas most affected by hail are those carried out by Font (1983). In them it was observed that in certain areas of the Ebro valley the frequency of storms reaches the value of 32 days of

storm per year. Similarly, the work carried out by Pascual (2002) evinces an average hailstorm frequency of 9.4 hail per year between the months of May and September in the same region of the Ebro valley. More recent articles such as those of García Ortega et al., (2014) using radar observations in the central area of the Ebro valley (≈ 60.000 km²) detect an annual average of 32.6 days of hail for the period 2001-2010. In the province of Lleida (Spain), over an area of 3500 km², 12 hail days per year were observed during the period 1995-2007 (Pascual, 2002; Farnell et al., 2009). In the Lleida observatory, a frequent place for hail episodes, Sousa (1987) estimated values of 1.4 days per year throughout the period 1953-1980. Bernaldo (2009) related hail days observed in different places and damage caused in agriculture in the provinces of Burgos, Cuenca, Valladolid and Zaragoza. While in Zaragoza, in the Ebro valley, the highest annual percentages of losses with 2.3% were detected, following an interval of 8 days of hail, the province of Burgos, in the north of Castilla y León and with a similar number of stations, there were average losses of only 1.85% albeit being distributed over 54 hail days. In Portugal, large hailstorms are a rare phenomenon, mainly due to the prevalence of westerly winds from the Atlantic Ocean. In its state observation network, only 7 days with hail of size of 2 cm or larger are referenced over a period of 10 years, and yet values of 5 days per year of small hail (presumably including graupel) are observed in elevated areas of the north of the country (Font Tullot, 2000).

Within the extensive set of existing references about the relationship between hail episodes and associated synoptic situations, it is worth mentioning: Sioutas and Flocas (2003) study hail days in northern Greece over a period of 26 years (1976-2001), extracting and analyzing the most pivotal synoptic modes that generate hail in that area, finding that a short wave trough was the dominant situation in the generation of the phenomenon. Schemm et al., (2016) analyze hail data observed in Switzerland over a

12-year period (2002-2013). They conclude that the occurrence of hail in Switzerland is associated with the existence of a cold front at an atmospheric level of 700 hPa. Li et al., (2016) study hails episodes that occurred in central China between 1960 and 2012, using reanalysis data provided by NCEP/NCAR. They analyzed the atmospheric circulation patterns that generated these hail episodes and defined five synoptic patterns that explained the occurrence of hail in the area. These deduced patterns were deep trough at 500 and 850 mb and thermal low pressure at sea level. Aran et al., (2011), using as variables the average atmospheric pressure at sea level and the geopotential height at 500 hPa level, classify and group the synoptic patterns causing hail in Lleida (Spain). Researchers such as Simeonov and Giorgiev, 2003; Garcia-Ortega et al., 2007; Huth et al., 2008; Kunz et al., 2009; Philipp and Bartholy, 2010; Twardosz, 2010; Saa Requejo et al., 2011; Johnson and Sugden, 2014; Wapler and James, 2014; Melcón et al., 2017 and Slahi et al., 2018 have used various statistical tools to analyze and classify the most frequent atmospheric patterns that generate hail in different places and periods.

The main objectives of this study are, first and foremost, to obtain, through the combined use of the techniques of Principal Component Analysis (PCA) and Cluster Analysis (CA), those synoptic patterns that bring about episodes of severe hail (> 3 cm) in Spain. Secondly, the results obtained in the previous stage are employed to showcase the synoptic analysis of representative cases with their most pronounced meteorological characteristics.

2. Data sets and methods

Hail observation in Spain is carried out directly and continuously (24 hours) in a few observatories from the main network of the State Meteorological Agency (AEMet) that have its own trained staff. The rest of the network makes general observations from

06 to 18 UTC, with some singular exceptions, such as the case of airports, which extend observations beyond 18 UTC through with variable hours and depending on the time of year. This network is complemented by the secondary network, made up of collaborators who altruistically make climatological observations and whose data is not subject to the same quality controls as data from observatories with AEMet personnel, which causes great uncertainty in the data. To this, it must be added that during the summer months, some observatories of the secondary network cannot guarantee their activities due to the vacation periods. The aforementioned evidence indicates that analyzing hail data from the national observation network is a complex task both spatially and temporally, especially considering that given the brevity of the phenomenon, its ongoing observation becomes paramount.

In 2012, AEMet develops a Singular Atmospheric Observations Notification System (SINOBAS in Spanish) capable of collecting and making available to citizens information about the occurrence of certain phenomena that have been called singular. Among them are included intense wind phenomena (tornadoes, waterspouts, vortices streak, etc.), precipitation phenomena (hailstorms, singular snowfalls, sudden precipitation) or other particular phenomena such as avalanches, breaking waves or transitory variations in sea levels. All of them are characterized by being local, infrequent, of significant intensity and capable of causing high social impact. Through this database, created in line with the concepts of crowdsourcing or citizen science, AEMet collects information provided by any citizen about the occurrence of meteorological phenomena. Due to their scale, they may go unnoticed by conventional observation networks and remote sensing systems, but which have meteorological relevance and may cause a significant impact upon the population. SINOBAS (<https://sinobas.aemet.es>) has been

operational since April 2013, although it allows reporting not only recent events, but also historical episodes of interest, making it feasible to find records even before the release date. It is a consolidated tool for AEMet, which provides, thanks to citizens' collaboration, valuable information that could otherwise be lost. It likewise establishes a connection between those interested in the area that concerns the monitoring of weather and atmospheric phenomena. AEMet technicians subsequently validate all the information entered into the system. That being so, it is gradually becoming a valuable database of unique meteorological phenomena that would otherwise be difficult to pinpoint and locate.

Of all the phenomena referenced in SINOBAS, we have selected the phenomenon of hail for it presents great economic and social impact, in addition to having associated peculiar atmospheric characteristics. From 2012 to 2019, 256 singular hailstorms were reported in SINOBAS by private citizens and subsequently validated by AEMet technicians. Of all of them, we have selected those hailstorms where the size of the hail was equal to or greater than 3 cm, as they constitute the events with the greatest environmental impact. Hence, a sample of 73 events has been obtained (from April to October as it is the annual period with the highest convective activity), something considered highly reliable. In Figure 1, we can observe the spatial distribution of the 73 analyzed events and it is necessary to indicate that the areas or places where no event is referred do not depend upon the absence of hail possibility, but rather on the absence of information provided by citizens, thus highlighting the areas and places where the citizens' interest in these phenomena is most pronounced.

The atmospheric variables used, both to classify and group the 73 selected episodes and to identify the characteristics and independent patterns or modes of

variability of set of data, were obtained by ERA-5 reanalysis by European Centre for Middle Range Weather Forecasting (ECMWF) (Dee et al., 2011). [https://www.ecmwf.int/en/forecasts/datasets/reanalysis-datasets/era5]

The methodological approach employed in this study consisted of applying Principal Component Analysis (PCA) coupled with Cluster Analysis (CA) as other authors have done (Richman, 1986; Yarnal, 1993). To apply these statistical techniques in a spatial domain it is necessary to use a continuous variable that provides the main dynamic and thermal structures. So, two indices were selected: a) one associated with the moisture flux at the 850 hPa pressure level, $(qv)_{850}$ (calculated by multiplying the mixing ratio and the wind intensity, units g m/kg s), and b) the lifted index (LI) (Galway, 1956), computed taking 500 hPa as the upper limit. These parameters were chosen because the supply of moisture at low levels and static instability are two key factors in the generation of heavy hail, (as commented in the Introduction). Consequently, they significantly explain the characteristics of the selected episodes in the sample of the 73 events. In any case, it should be taken into account that there are other relevant factors in the determination of the final amount of hail and its location, such as orography and low-level convergence. The 850 hPa pressure level was selected because it is representative of low levels and in general without being subject to local effects except in some reduced areas of the domain studied. As Huth et al., (2008) indicate, the use of PCA in the classification of synoptic patterns is twofold. In our analysis, PCA is used prior to CA, so it cannot be considered a classification tool because the posterior CA accomplishes this aim. The PCA is only used as an intermediate tool for the data dimension reduction.

The PCA was applied to the covariance matrix of these indices, and the resulting empirical orthogonal functions/patterns (EOF) were of unit variance and, also, were not

rotated. It should be noted that there is a little correlation between the two parameters ($r = 0.01$), and they can therefore be regarded as lineally independent. Accordingly, only one principal component was retained, which explained 62.7% of the total variance. Later, CA is applied to the factor scores resulting from the PCA. The clustering algorithm used is the non-hierarchical K-means method. For this algorithm the number of the groups is required beforehand. This can be decided by taking into account the results of a procedure called “jump method”. This procedure is calculated from a hierarchical clustering algorithm and using the Ward Method as an agglomeration technique. The coefficient given in the agglomeration schedule turns out to be the within-cluster sum of squares at each step. The number of groups is estimated detecting the greater distortion between the coefficients in two consecutive steps. Finally, the K-means method is used without iterative steps. These approaches have been widely applied in atmospheric studies and are described in minute detail in many textbooks (e.g. Wilks, 2006). The application of this procedure gave 4 groups with their respective final cluster center, which represents for each case, the final cluster assignment made from the Euclidean distance between the case and the cluster center used to classify the case. We take as the characteristic pattern of each cluster, the case closest to each final cluster center.

3. Results and discussion

The spatial distribution of the 73 hail events with size $\geq 3\text{cm}$ is evinced in Figure 1. Most of observed cases were associated with mountain ranges, especially the Sistema Iberico. This fact was also reported by García Ortega et al. (2012) and it is due to the flow perturbations caused by the mountain, since the upslope flow contributes to trigger and maintain deep convection (de la Torre et al., 2015). The impact of orography in hail

was regarded all over the world (for example Punge et al., 2014 in the Massif Central in France, de la Torre et al., 2015 in Los Andes; Nisi et al., 2016 in the Alps). Figure 1 also elucidates that areas close the North and East coasts presented high density of severe hail events. This is in agreement with the outcome provided by Sánchez et al., (2003). The presence of moisture at low levels becomes a staple ingredient for deep convection (Markowski and Richardson, 2010) and, consequently, moisture flux from the Cantábrico and Mediterranean seas favour the development of hailstorm.

Table 1 shows that ~ 74% of the severe hail events considered in this study occurred between July and September. Most of studies in Europe reported that hail is observed namely between April and September (see Punge and Kunz, 2016 and references herein). The high surface temperature during the warm season provides an appropriate thermodynamic atmospheric background for convection. Hailstorm formation need high static instability and sufficient moisture supply at low levels (Markowski and Richardson, 2010). As expected, both requirements were met in the hail events considered in this study. The average values of moisture flux and LI were 66.8 g m/kg s and – 3.6 respectively.

The application of the procedure indicated in the item 2 gave 4 groups or clusters. The case closest to each final cluster centre was taken as the characteristic of each cluster. As expected, the four cluster centers presented values of moisture flux and LI greater than average (see Table 2).

Group 1 (13 cases. Cluster centre : Alagón, 31/07/2015)

A geopotential and thermal trough at the 500 hPa pressure level (Fig. 2a) with axis over Portugal was going through the Iberian Peninsula (IP). The pattern at sea level showed the Azores anticyclone over the Atlantic ocean with a low over the IP. Low level flow was from SE in the east IP. Temperature was high, ~ 24°C at 850 hPa (Fig.

2b). Moreover, the water content in the IP was high, especially eastern IP with ~ 45 kg/m² in the zone of the cluster center (Fig.3a). This synoptic environment was favorable for deep convection. As a result, severe hail was mainly reported on the east face of Sistema Ibérico. The model sounding (Fig.3b) for the cluster center conveyed high values of surface-based CAPE (SBCAPE = 563 J/kg) and great thickness for convection (more than 10000 m). The sounding gave high values of shear, storm relative helicity (~ 240 m²/s²), and precipitable water. The satellite and radar images (Fig. 4a and b) manifested organized convection in the SW-NE direction, probably due to forcing associated with the 500 hPa trough. The cold tops of cumulonimbus (CB) indicated deep convection and reflectivity values 54 dBz, which were representative of large hail.

Group 2 (18 cases, cluster center : Tineo, 22/6/2016)

A geopotential and thermal trough at 500 hPa were seen entering the northwestern IP (Fig 5a). Low pressure was over the IP at the sea level, with flow from SW in the east half of the IP. Temperature at 850 hPa was high: ~24°C in the central IP (Fig. 5b). There was a lot of water content, peaking over the north IP (Fig. 6a). These synoptic conditions were appropriate for deep convection to develop. Severe hail associated with this group tended to be found south of the mountains. The model sounding for the cluster center (Fig. 6b) reveals high static instability (SBCAPE = 627 J/kg). There was a small inversion at the surface, so some forcing as heating of wind convergence was necessary to trigger convection. In this case the thickness for convection was 12000 m. Shear was high, but storm relative helicity was moderate (66 m²/s²). The satellite image (Fig. 7a) exposed deep convection that seem to be organized as a mesoscale convective system. Reflectivity values were > 54 dBz, even over 60 dBz in some zones, which were values compatible with large hail (Fig. 7b).

276 Group 3 (6 cases, cluster center: La Paúl, 13/9/2019)

277 A trough affecting the NW of the IP was seen at the 500 hPa pressure level.
278 There was also cold air at mean and high levels over the northwestern IP, with
279 temperature of $\sim -20^{\circ}\text{C}$ at 500 hPa (Fig. 8a) A low pressure centered over the SW of
280 France affecting the northern IP appeared at the surface level. Temperature at low levels
281 was high: 20°C at the 850 pressure level (Fig. 8b). High water content appeared over the
282 northern and eastern IP, with values $\sim 35 \text{ kg/m}^2$ in the zone of the cluster center (Fig.
283 9a). Low level flow was from W/NW. This was the group with the fewest number of
284 severe hail cases detected, all of them in the east half of the IP. The model sounding
285 (Fig. 9b) revealed high static instability ($\text{SBCAPE} = 642 \text{ J/kg}$), great thickness for
286 convection (10500 m), and high values of shear and storm relative helicity ($191 \text{ m}^2/\text{s}^2$).
287 Satellite image (Fig. 10a) showcased cloud bands in front of the low in northern Spain
288 and southern France. The most salient convective development was perceived in
289 Aragon and Navarra. Reflectivity values (Fig. 10b) were $> 60 \text{ dBz}$ in the zone of the
290 cluster centre.

291 Group 4 (36 cases, cluster centre: Castellfort, 29/7/2015)

292 Zonal flow over the north half of the IP and high pressures on the SW of the IP
293 were scrutinized at the 500 hPa, with temperatures $\sim -8^{\circ}\text{C}$ in the study area (Fig. 11a).
294 Two high pressure centres were observed on the Atlantic Ocean and the Cantábrico Sea
295 at surface level, with relative low pressures in the east half of the IP. Low level
296 temperature was high ($\sim 28^{\circ}\text{C}$ at the 850 hPa pressure level) (Fig. 11b). The water
297 content was also high, with values $> 40 \text{ kg/m}^2$ in the study area (Fig. 12a). Low level
298 flow was from SW. This was the cluster presenting the highest number of reported
299 events of severe hail. Most of them were located at the north and east of the IP. The
300 model sounding (Fig. 12b) revealed noticeable static instability ($\text{CAPE} = 2385 \text{ J/kg}$)

and thickness for convection (12500 m). Moreover, the values of shear and helicity were high. Satellite image (Fig.13a) conveyed convective development over the Mediterranean coast. It is remarkable the mesoscale convective system over the cluster centre. Reflectivity values were > 60 dBz in that zone (Fig. 13b).

The aforementioned synoptic conditions associated with severe hail in Spain encountered in this study are in accordance with those reported in sundry regions and countries in Europe: trough at mean levels of the atmosphere and low pressure and fronts with warm and moist air at low levels (for example Aran et al., 2011; Twardosz et al., 2010; Garcia Ortega et al., 2011; Kapsch et al., 2012; Berthet et al., 2013). Many studies have suggested that hail occurrence is related to high CAPE values and moderate or strong shear and substantial storm relative helicity (Craven and Brooks, 2004; Groenemeijer and van Delden, 2007; Púčik et al., 2015; Kunz et al., 2017). This is also found in the cases of severe hail in the IP.

4. Conclusions

In this study, 73 events of severe hail (size ≥ 3 cm) - observed in Spain in the period 2012 to 2019 – have been analyzed. Most of these events tend to be concentrated in mountainous areas, markedly on mountainside terrain facing the Mediterranean and Cantábrico seas from July to September. The 73 episodes were classified relying upon a Principal Component Analysis (PCA) coupled with K-mean clustering and four synoptic types were distinguished. Two indices were employed to carry out this classification: moisture flux at the 850 hPa pressure level and the Lifted Index and the characteristic patterns of each group are represented by the patterns of the cluster centers. These two variables, uncorrelated with one another, have a strong influence on heavy hailstorm, although the final amount is modulated by certain factors, some of

1
2
3
4
5
6
7
8
9
10
11
12
13
14
15
16
17
18
19
20
21
22
23
24
25
26
27
28
29
30
31
32
33
34
35
36
37
38
39
40
41
42
43
44
45
46
47
48
49
50
51
52
53
54
55
56
57
58
59
60
61
62
63
64
65

326 them with very local influences, such as mechanisms of convergence at low levels,
327 orographic interaction, and the persistence of a proper flow. The importance of the
328 propagation characteristics of precipitating systems, due to various meso and microscale
329 factors, should also be emphasized.

330 The ensuing main conclusions are to be extracted from the meteorological
331 conditions associated with each cluster:

332 (i) In the sample of the 73 cases studied, high values of low level moisture flux
333 ($\sim 89 \text{ g m/kg s}$ on the average) were seen accompanied by static instability (SBCAPE \sim
334 600 J/kg and average LI ~ -4).

335 (ii) The most typical configuration correspond to geopotential and thermal
336 trough at mean levels of the troposphere and low pressure at low levels.

337 (iii) The temperature values exceed 20°C at the 850 hPa pressure level and
338 range between -8°C and -20°C at the 500 hPa pressure level.

339 (iv) High values of precipitable water have been detected ($> 35 \text{ kg/m}^2$).

340 (v) The presence of storm relative helicity and shear was moderate or strong in
341 all cases.

342 Information on hail events (with size $\geq 3\text{cm}$) characteristics from SINOBAS
343 data set (AEMet) has been evaluated with the objective to present an overview of
344 knowledge on severe hailstorms across Spain. It is worth mentioning here that the
345 observed meteorological conditions are in line with those uncovered in other studies in
346 Europe and dissimilar regions.

347 348 **ACKNOWLEDGMENTS**

349 The authors thank the Spanish State Meteorological Agency (AEMet) for
350 providing the hail data, the European Centre for Medium-Range Weather Forecasts

(ECMWF) for allowing the information on their website to be used and the Service of Geographical Information (STIG)-Nucleus of the University of Salamanca for its assistance in mapping the layouts.

REFERENCES

Aran, M., Pena, J., Torá, A., 2011. Atmospheric circulation patterns associated with hail events in Lleida (Catalonia); Atmos. Res. 100 428–438.

<https://doi.org/10.1016/j.atmosres.2010.10.029>

Bernaldo, I., 2009. Estudio de la evolución e intensidad de los daños por granizo en trigo y cebada. Tech. Rep. Departamento de Matemática Aplicada a la Ingeniería Agronómica, Universidad Politécnica de Madrid.

Berthet, C., Wesolek, E., Dessens, J., Sánchez, J.L., 2013. Extreme hail day climatology in southwestern France. Atmos. Res. 123, 139–150.

<https://doi.org/10.1016/j.atmosres.2012.10.007>

Burgaz, F., 2004. Experiencia española. IICA Biblioteca Venezuela, Santiago, Chile
URL <https://books.google.de/books?id=3zwqAAAAYAAJ>.

Craven, J.P., Brooks, H.E., 2004. Baseline climatology of sounding derived parameters associated with deep, moist convection. Nat. Weather Dig. 28, 13–24.

de la Torre, A., Pessano, H., Hierro, R., Santos, J., Llamado, P., Alexander, P., 2015. The influence of topography on vertical velocity of air in relation to severe storms near the southern Andes Mountains. Atmos. Res. 156, 91–101. <https://doi.org/10.1016/j.atmosres.2014.12.020>

Dee, D.P., Uppala, S.M., Simmons, A.J., Berrisford, P., Poli, P., Kobayashi, S., Andrae, U., Balmaseda, M.A., Balsamo, G., Bauer, P., Bechtold, P., Beljaars, A.C.M., van de Berg, L., Bidlot, J., Bormann, N., Delsol, C., Dragani, R., Fuentes, M., Geer, A.J.,

376 Haimberger, L., Healy, S.B., Hersbach, H., Hólm, E.V., Isaksen, I., Kállberg, P.,
 377 Köhler, M., Matricardi, M., McNally, A.P., Monge-Sanz, B.M., Morcrette, J.-J., Park,
 378 B.-K., Peubey, C., de Rosnay, P., Tavolato, C., Thépaut, J.-N., Vitart, F. 2011. The ERA-
 379 Interim reanalysis: configuration and performance of the data assimilation system. Q. J.
 380 R. Meteorol. Soc. 137: 553–597. <https://doi.org/10.1002/qj.828>
 381 Farnell, C., Busto, M., Aran, M., Andres, A., Pineda, N., Torá, M., 2009. Estudio de la
 382 granizada del 17 de septiembre de 2007 en el Pla d’Urgell, primera parte: trabajo de
 383 campo y análisis de los granizómetros. Tethys 6, 69–81 (in Spanish).
 384 Font, I., 1983. Atlas Climático de España. INM y Ministerio de Transportes. Turismo y
 385 Comunicaciones, Madrid. 296 pp.
 386 Font Tullot, I., 2000. Climatología de España y Portugal. Acta Salmanticensia.
 387 Ediciones Universidad de Salamanca URL <https://books.google.de/books?id=Uf46Uka->
 388 ViAC.
 389 Galway, J.G., 1956. The Lifted Index as a Predictor of Latent Instability. Bulletin of the
 390 American Meteorological Society, 37, 528-529.
 391 García-Ortega, E., Fita, L., Romero, R., Lopez, L., Ramis, C., Sanchez, J.L., 2007.
 392 Numerical simulation and sensitivity study of a severe hailstorm in northeast Spain;
 393 Atmos. Res. 83 225–241. <https://doi.org/10.1016/j.atmosres.2005.08.004>
 394 García-Ortega, E., López, L., Sánchez, J., 2011. Atmospheric patterns associated with
 395 hail- storm days in the Ebro Valley, Spain. Atmos. Res. 100 (4), 401–427.
 396 <https://doi.org/10.1016/j.atmosres.2010.08.023>
 397 García-Ortega, E., Merino, A., López, L., Sánchez, J.L., 2012. Role of mesoscale
 398 factors at the onset of deep convection on hailstorm days and their relation to the
 399 synoptic patterns. Atmos. Res. 114-115 (0), 91–106. <https://doi.org/10.1016/j.atmosres.2012.05.017>
 400

401 García-Ortega, E., Hermida, L., Hierro, R., Merino, A., Gascón, E., Fernández-
 402 González, S., Sánchez, J., López, L., 2014. Anomalies, trends and variability in
 403 atmospheric fields related to hailstorms in north-eastern Spain. *Int. J. Climatol.* 34 (11),
 404 3251–3263. [https://doi.org/ 10.1002/joc.3910](https://doi.org/10.1002/joc.3910)
 405 Groenemeijer, P.H., van Delden, A., 2007. Sounding-derived parameters associated
 406 with large hail and tornadoes in the Netherlands. *Atmos. Res.* 83 (2-4), 473–487.
 407 [https://doi.org/ 10.1016/j.atmosres.2005.08.006](https://doi.org/10.1016/j.atmosres.2005.08.006)
 408 Huth, R., Beck, C., Philipp, A., Demuzere, M., Ustrnul, Z., Cahynová, M., Kyselý, J.
 409 and Tveito, O.E. 2008. Classifications of atmospheric circulation patterns. Recent
 410 advances and applications. Trends and directions in climate research. *Annals of the N.Y.*
 411 *Academy Sciences*, 1146, 105–152. <https://doi.org/10.1196/annals.1446.019>.
 412 Johnson, A.W., Sugden, K.E., 2014. Evaluation of sounding derived thermodynamic
 413 and wind-related parameters associated with large hail events; *EJSSM* 9(5) 1–42.
 414 Kapsch, M.-L., Kunz, M., Vitolo, R., Economou, T., 2012. Long-term trends of hail-
 415 related weather types in an ensemble of regional climate models using a bayesian
 416 approach. *J. Geophys. Res. D: Atmos.* 117 (15). [https://doi.org/ 10.1029/2011JD017185](https://doi.org/10.1029/2011JD017185)
 417 Kunz, M., Sander, J., Kottmeier, C., 2009. Recent trends of thunderstorm and hailstorm
 418 frequency and their relation to atmospheric characteristics in southwest Germany; *Int. J.*
 419 *Climatol.* 29 2283–2297. [https://doi.org/ 10.1002/joc.1865](https://doi.org/10.1002/joc.1865)
 420 Kunz, M., Blahak, U., Handwerker, J., Schmidberger, M., Heinz Jürgen Punge, H.,
 421 Mohr, S., Fluck, E., Bedka, K.M., 2017. The severe hailstorm in southwest Germany on
 422 28 July 2013: characteristics, impacts and meteorological conditions. *Q. J. R. Meteorol.*
 423 *Soc.* <https://doi.org/10.1002/qj.3197>.

424 Li, M., Zhang, Q., Zhang, F., 2016. Hail day frequency trends and associated
 425 atmospheric circulation patterns, over China during 1960–2012; *J. Climate* 29 7027–
 426 7044. <https://doi.org/10.1175/JCLI-D-15-0500.1>
 427 Markowski, P., Richardson, Y., 2010. *Mesoscale Meteorology in Midlatitudes*. John
 428 Wiley & Sons, Ltd. <http://doi.org/10.1002/9780470682104>.
 429 Melcón, P., Merino, A., Sánchez, J.L., López, L., García-Ortega, E., 2017. Spatial
 430 patterns of thermodynamic conditions of hailstorms in southwestern France. *Atmos. Res.*
 431 189, 111–126. <https://doi.org/10.1016/j.atmosres.2017.01.011>.
 432 Nisi, L., Martius, O., Hering, A., Kunz, M., Germann, U., 2016. Spatial and temporal
 433 distribution of hailstorms in the Alpine region: a long-term, high resolution, radar-based
 434 analysis. *Q. J. Roy. Meteorol. Soc.* 142, 697. <http://doi.org/10.1002/qj.2771>.
 435 Pascual, R., 2002. Granizo en el llano de Lleida. Note 11 p. Agencia Estatal de
 436 Meteorología, Madrid. Spain. (ModulosTempo, available at: <http://www.aemet.es/>).
 437 Philipp, A., Bartholy, J., 2010. COST733CAT-A database of weather and circulation
 438 type classifications; *Phys. Chem. Earth.* 35 360–373.
 439 <https://doi.org/10.1016/j.pce.2009.12.010>
 440 Porras, I., Sairouni, A., Aran, M., 2013. Climatología de la probabilitat de calamarsa a
 441 Catalunya. [in Catalan]. URL [http://static-m.meteo.cat/wordpressweb/wp-content/](http://static-m.meteo.cat/wordpressweb/wp-content/uploads/2014/11/18130754/nota-estudi-climatologia-calamarsa-n74.pdf)
 442 [uploads/2014/11/18130754/nota-estudi-climatologia-calamarsa-n74.pdf](http://static-m.meteo.cat/wordpressweb/wp-content/uploads/2014/11/18130754/nota-estudi-climatologia-calamarsa-n74.pdf).
 443 Púčik, T., Groenemeijer, P., Rýva, D., Kolář, M., Proximity Soundings of Severe and
 444 Nonsevere Thunderstorms in Central Europe. *Mon. Wea. Rev.* (2015) 143 (12): 4805–
 445 4821. <https://doi.org/10.1175/MWR-D-15-0104.1>.
 446 Punge, H.J., Kunz, M., 2016. Hail observations and hailstorm characteristics in Europe:
 447 A review. *Atmos. Res.* 176–177, 159–184.
 448 <https://doi.org/10.1016/j.atmosres.2016.02.012>

449 Punge, H., Bedka, K., Kunz, M., Werner, A., 2014. A new physically based stochastic
 450 event catalog for hail in Europe. *Nat. Hazards* 73 (3), 1625–1645. [https://doi.org/](https://doi.org/10.1007/s11069-014-1161-0)
 451 10.1007/s11069-014-1161-0
 452 Richman, M.B., 1986. Rotation of Principal Components. *J. Climatol.* 6, 293–335.
 453 <https://doi.org/10.1002/joc.3370060305>
 454 Saa Requejo, A., García Moreno, R., Díaz Alvarez, M.C., Burgaz, F., Tarquis, M., 2011.
 455 Analysis of hail damages and temperature series for peninsular Spain. *Nat. Hazards*
 456 *Earth Syst. Sci.* 11 (12), 3415–3422 URL [http://www.nat-hazards-earth-syst-sci.net/11/](http://www.nat-hazards-earth-syst-sci.net/11/3415/2011/)
 457 3415/2011/.
 458 Salahi, B., Nohegar, A., Behrouzi, M., Aalijahan, M., 2018. Synoptic patterns leading to
 459 hailstorm in Chaharmahal and Bakhtiari province, Iran. *Journal of Earth System Science.*
 460 127,23. <https://doi.org/10.1007/s12040-018-0924-5>.
 461 Sánchez, J.L., Fernández, M.V., Fernández, J.T., Tuduri, E., Ramis, C., 2003. Analysis
 462 of mesoscale convective systems with hail precipitation. *Atmos. Res.* 67–68, 573–588.
 463 [https://doi.org/ 10.1016/S0169-8095\(03\)00074-7](https://doi.org/10.1016/S0169-8095(03)00074-7)
 464 Schemm, S., Nisi, L., Martinov, A., Leuenberger, D., Martius, O., 2016. On the link
 465 between cold fronts and hail in Switzerland; *Atmos. Sci. Lett.* 17(5) 315–325.
 466 [https://doi.org/ 10.1002/asl.660](https://doi.org/10.1002/asl.660)
 467 Simeonov, P., Giorgiev, C.G., 2003. Severe wind/hail storms over Bulgaria in 1999–
 468 2001 period: Synoptic- and meso-scale factors for generation. *Atmos. Res.* 67–68 629–
 469 643. [https://doi.org/ 10.1016/S0169-8095\(03\)00077-2](https://doi.org/10.1016/S0169-8095(03)00077-2)
 470 Sioutas, M., Flocas, H., 2003. Hailstorms in northern Greece: synoptic patterns and
 471 thermodynamic environment. *Theor. Appl. Climatol.* 75 (3), 189–202. [https://doi.org/](https://doi.org/10.1007/s00704-003-0734-8)
 472 10.1007/s00704-003-0734-8

473 Sousa, R., 1987. Notas para una climatología de Lérida. Instituto Nacional de
 474 Meteorología, Madrid (in Spanish).
 475 SwissRe, 2014. Sigma: Natural- and Man-made Catastrophes 2013. Tech. Rep. Swiss
 476 Re Economic Research and Consulting.
 477 Twardosz, R., 2010. A synoptic analysis of the diurnal cycle of thunderstorm
 478 precipitation in Kraków (southern Poland); Int. J. Climatol. 30 1008–1013.
 479 [https://doi.org/ 10.1002/joc.1960](https://doi.org/10.1002/joc.1960)
 480 Twardosz, R., Niedzwiedz, T., Łupikasz, E., 2010. Hail thunderstorms in Kraków and
 481 their circulation determinants (1863–2008). Woda w badaniach geograficznych. Instytut
 482 Geografii Uniwersytet Jana Kochanowskiego, Kielce, pp. 295–305.
 483 Wapler, K., James, P., 2014. Thunderstorm occurrence and characteristics in central
 484 Europe under different synoptic conditions; Atmos. Res. 158 1–14. [https://doi.org/](https://doi.org/10.1016/j.atmosres.2014.07.011)
 485 [10.1016/j.atmosres.2014.07.011](https://doi.org/10.1016/j.atmosres.2014.07.011)
 486 Wilks, D.S., 2006. Statistical methods in the atmospheric sciences, 2nd ed. International
 487 Geophysics Series, vol. 59. Academic Press (627 pp).
 488 Yarnal, B., 1993. Synoptic climatology in environmental analysis. Belhaven Press,
 489 London. 195 pp. <https://doi.org/10.1177/030913339401800422>
 490 Zimmerli, P., 2005. Hailstorms in Europe - A New Look at a Familiar Risk, Swiss Re
 491 Fokus Report, Zurich.

498

Hail days	2012	2013	2014	2015	2016	2017	2018	2019	Month	%
									total	month
April	0	0	0	0	0	1	0	0	1	1.37
May	0	0	0	3	0	0	4	0	7	9.59
June	1	3	4	2	1	4	3	0	18	24.66
July	1	2	0	7	0	7	4	3	24	32.87
August	0	0	1	4	1	3	2	1	12	16.44
September	0	0	2	2	1	1	3	0	9	12.32
October	0	1	0	0	0	1	0	0	2	2.75
Annual	2	6	7	18	3	17	16	4	73	
total										
% annual	2.73	8.22	9.59	24.65	4.12	23.29	21.91	5.49		

499

500 Table 1. Annual and month percentages of the 73 selected hail events between April and
501 October 2012–2019.

502

503

504

505

506

507

15
16
17
18
19
20
21
22
23
24
25
26
27
28
29
30
31
32
33
34
35
36
37
38
39
40
41
42
43
44
45
46
47
48
49
50
51
52
53
54
55
56
57
58
59
60
61
62
63
64
65

Cluster	Year	Month	Day	Location	Latitude	Longitude	Altitude	(qv) ₈₅₀	LI
			(Hour)		(N)	(E)	(m)	[g kg ⁻¹ m s ⁻¹]	
			(UTC)						
1	2015	July	31	Alagón (Zaragoza)	41.7724	-1.1189	228	99.78	-4.8
			(13.15)						
2	2016	June	22	Tineo (Asturias)	43.3321	-6.4144	568	41.42	-1.8
			(17.30)						
3	2016	September	13	La Paúl (Huesca)	41.9851	-0.7870	321	184.73	-4.8
			(15.30)						
4	2015	July	29	Castellfort	40.5030	-0.1912	1151	30.16	-4.5
			(15.15)	(Castellón)					

Table 2. Characteristics and location of the cluster centers selected by the PCA and CA statistical analysis.

Figure captions.

Figure 1. Geographical characteristics and location of the 73 hail events with size $\geq 3\text{cm}$ used in this study, indicating (star) the cluster centers.

Figure 2. Weather charts for group I (Cluster centre: Alagón, 31/07/2015, 13 UTC): (a) geopotential height (m) and temperature ($^{\circ}\text{C}$) at the 500 hPa pressure level; (b) mean sea-level pressure (hPa) and temperature ($^{\circ}\text{C}$) at the 500 hPa pressure level.

Figure 3. Weather charts for group I (Cluster centre: Alagón, 31/07/2015, 13 UTC): (a) Total column water (kg/m^2); (b) Soundings interpolated by the deterministic model of the ECMWF for the cluster centre.

Figure 4. 31 July 2015: (a) Mesoscale convective system seen by Meteosat (IR channel), 12 UTC. (b) Radar image (dBz) plan position indicator (PPI) over zone by AEMet, 13 UTC.

Figure 5. Weather charts for group II (Cluster centre: Tineo, 22/06/2016, 17 UTC): (a) geopotential height (m) and temperature ($^{\circ}\text{C}$) at the 500 hPa pressure level; (b) mean sea-level pressure (hPa) and temperature ($^{\circ}\text{C}$) at the 500 hPa pressure level.

Figure 6. Weather charts for group II (Cluster centre: Tineo, 22/06/2016, 17 UTC): (a) Total column water (kg/m^2); (b) Soundings interpolated by the deterministic model of the ECMWF for the cluster centre.

Figure 7. 22 June 2016: (a) Mesoscale convective system seen by Meteosat (IR channel), 17 UTC. (b) Radar image (dBz) plan position indicator (PPI) over zone by AEMet, 17 UTC.

Figure 8. Weather charts for group III (Cluster centre: La Paúl, 13/09/2016, 15 UTC): (a) geopotential height (m) and temperature ($^{\circ}\text{C}$) at the 500 hPa pressure level; (b) mean sea-level pressure (hPa) and temperature ($^{\circ}\text{C}$) at the 500 hPa pressure level.

Figure 9. Weather charts for group III (Cluster centre: La Paúl, 13/09/2016, 15 UTC):

(a) Total column water (kg/m^2); (b) Soundings interpolated by the deterministic model of the ECMWF for the cluster centre.

Figure 10. 13 September 2016: (a) Mesoscale convective system seen by Meteosat (IR channel), 15 UTC. (b) Radar image (dBz) plan position indicator (PPI) over zone by AEMet, 15 UTC.

Figure 11. Weather charts for group IV (Cluster centre: Castellfort, 29/07/2015, 15 UTC): (a) geopotential height (m) and temperature ($^{\circ}\text{C}$) at the 500 hPa pressure level; (b) mean sea-level pressure (hPa) and temperature ($^{\circ}\text{C}$) at the 500 hPa pressure level.

Figure 12. Weather charts for group IV (Cluster centre: Castellfort, 29/07/2015, 15 UTC): (a) Total column water (kg/m^2); (b) Soundings interpolated by the deterministic model of the ECMWF for the cluster centre.

Figure 13. 29 July 2015: (a) Mesoscale convective system seen by Meteosat (IR channel), 15 UTC. (b) Radar image (dBz) plan position indicator (PPI) over zone by AEMet, 15 UTC

FIGURE 1

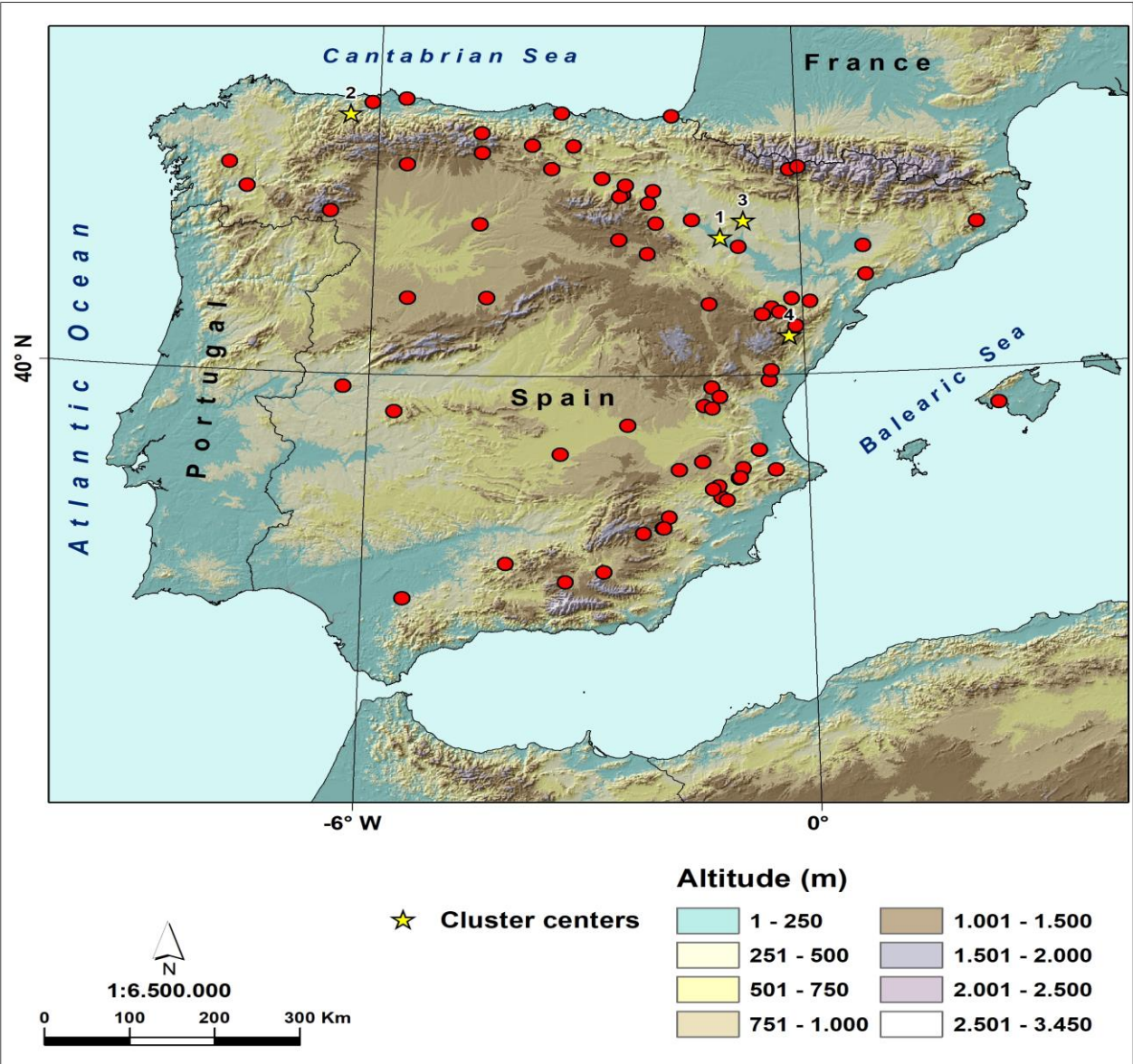
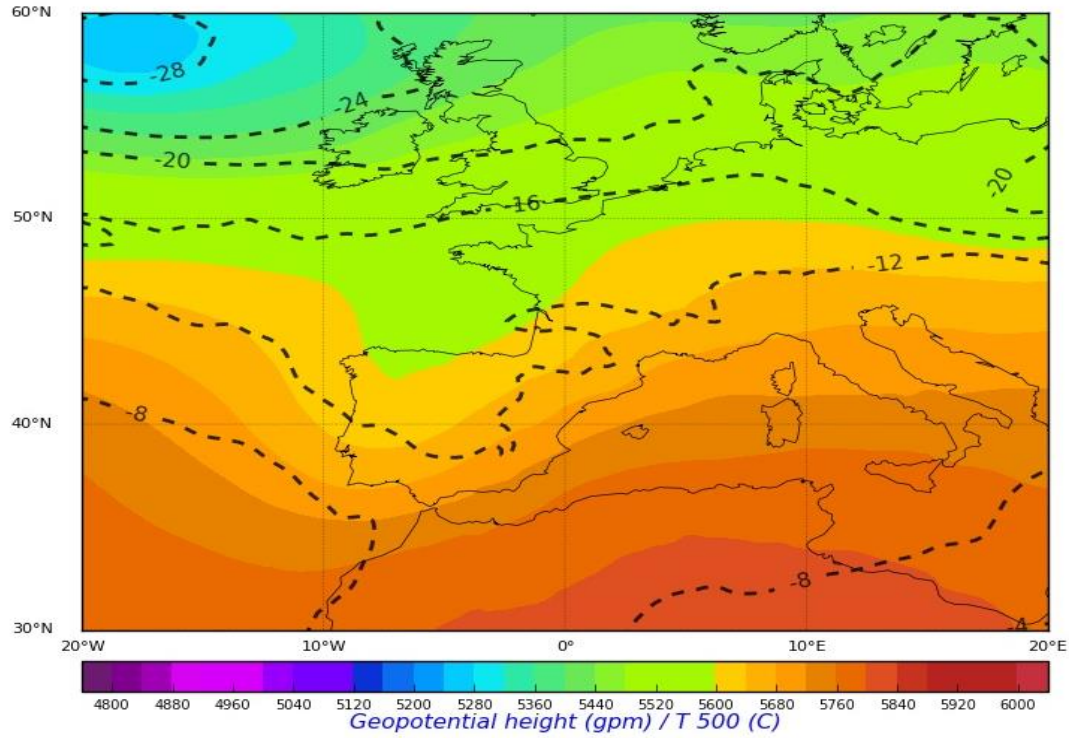


FIGURE 2

(a)



(b)

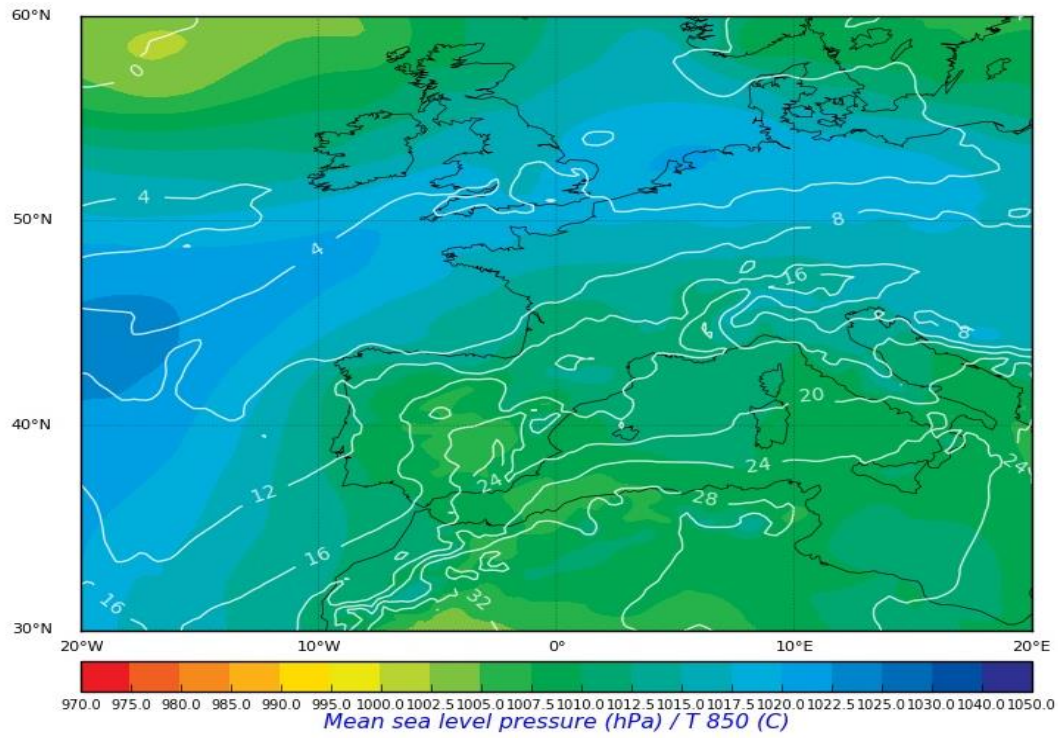
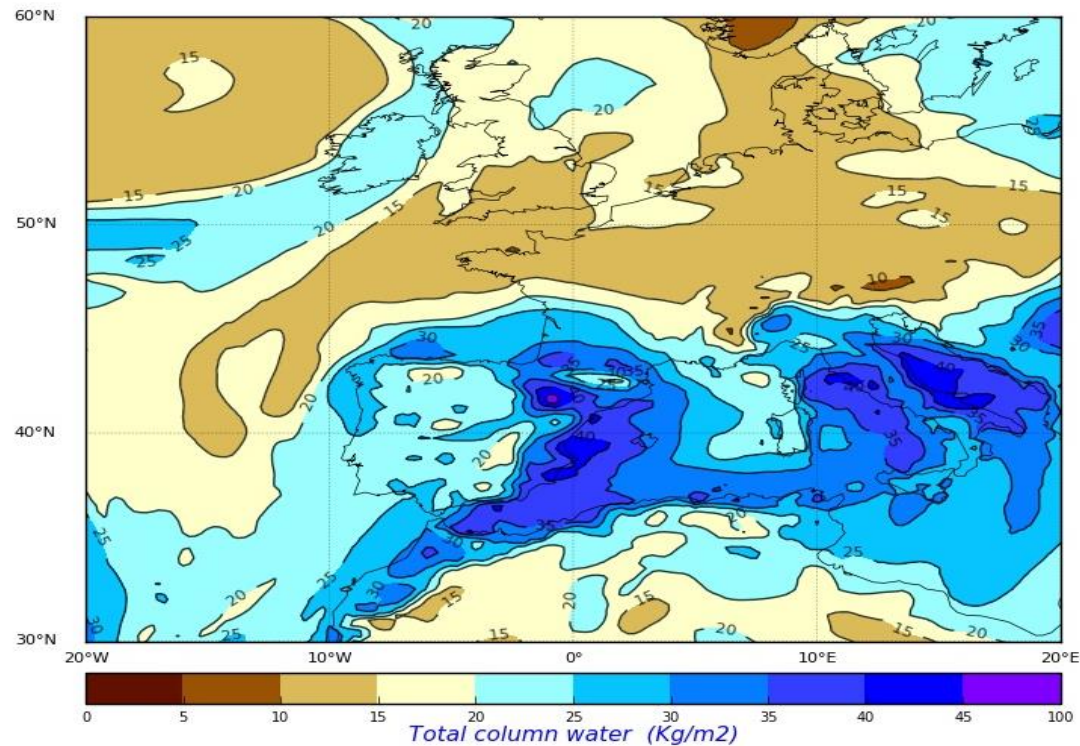


FIGURE 3

(a)



(b)

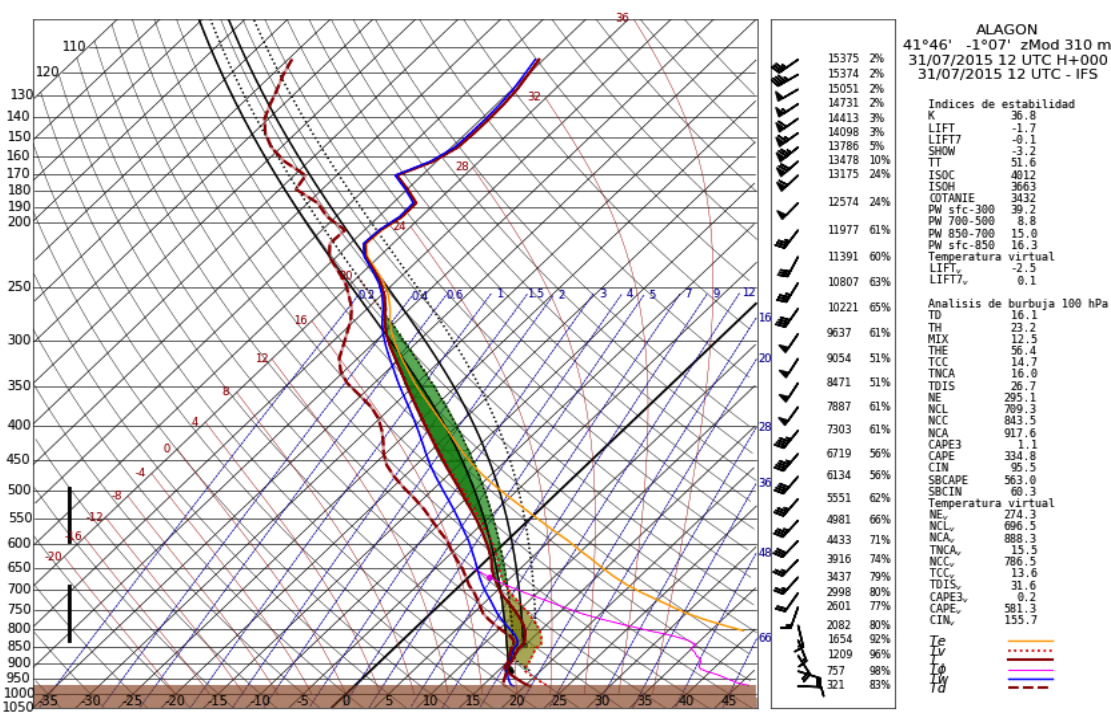
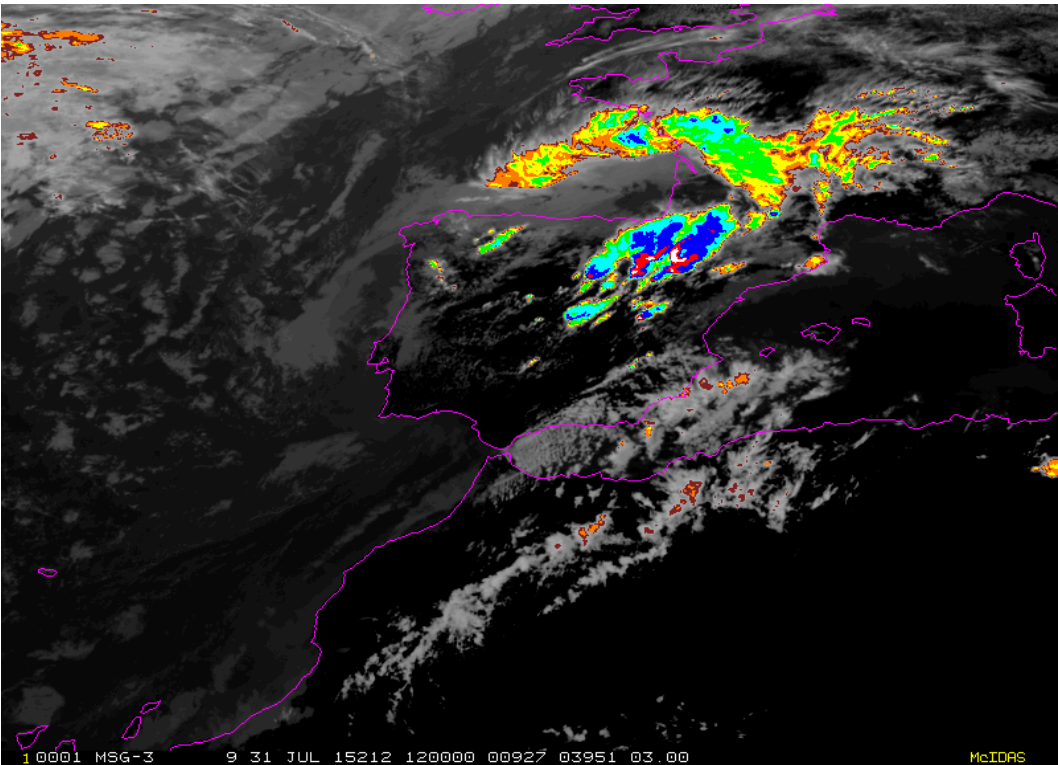


FIGURE 4

(a)



(b)

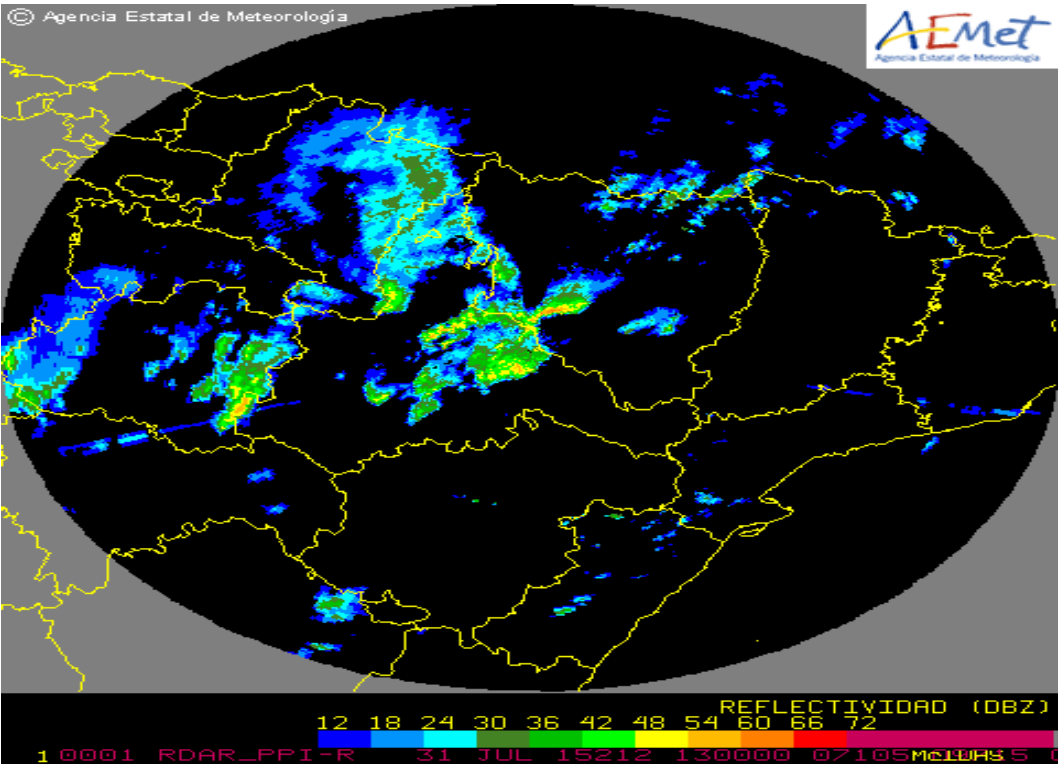
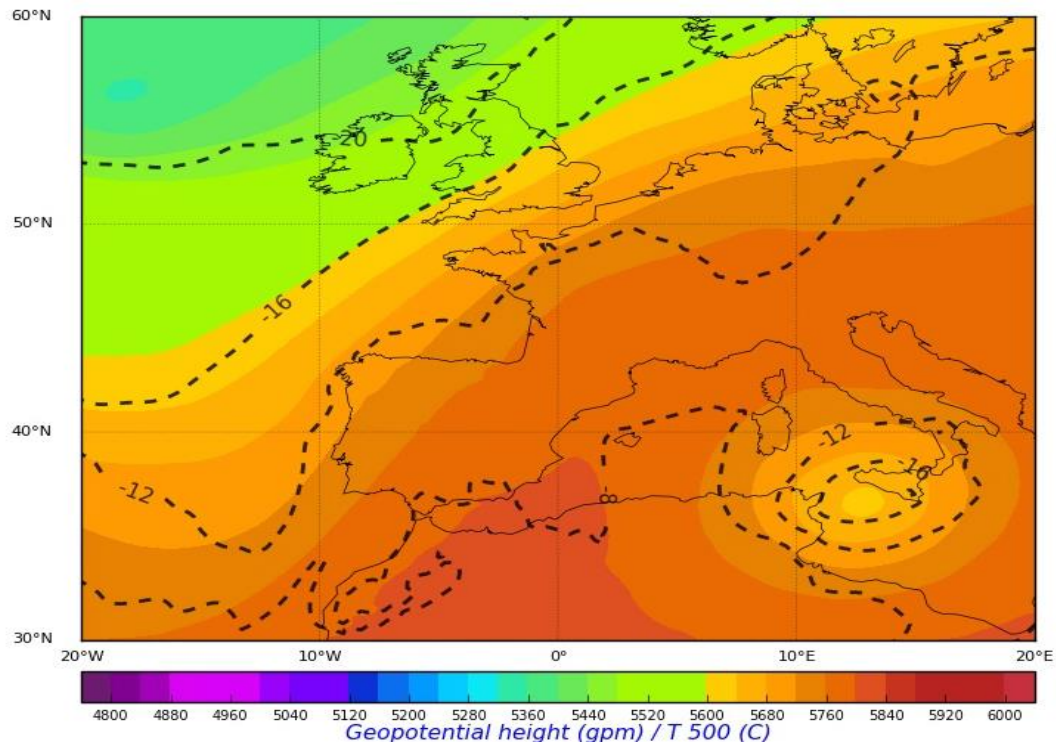


FIGURE 5

(a)



(b)

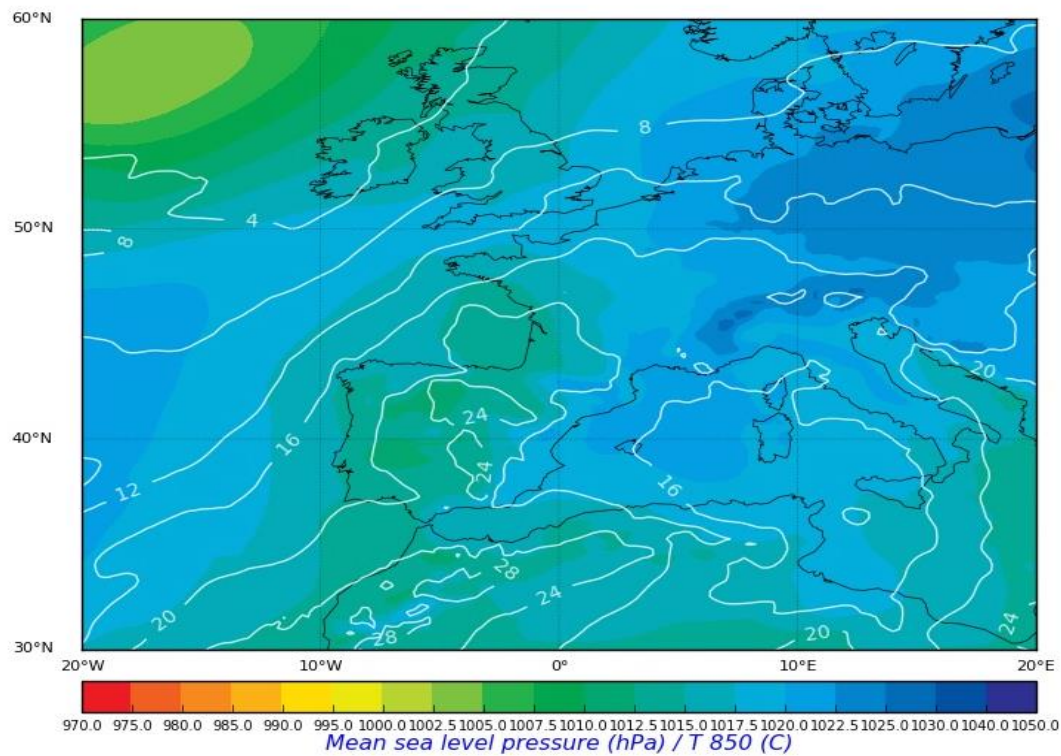


FIGURE 6

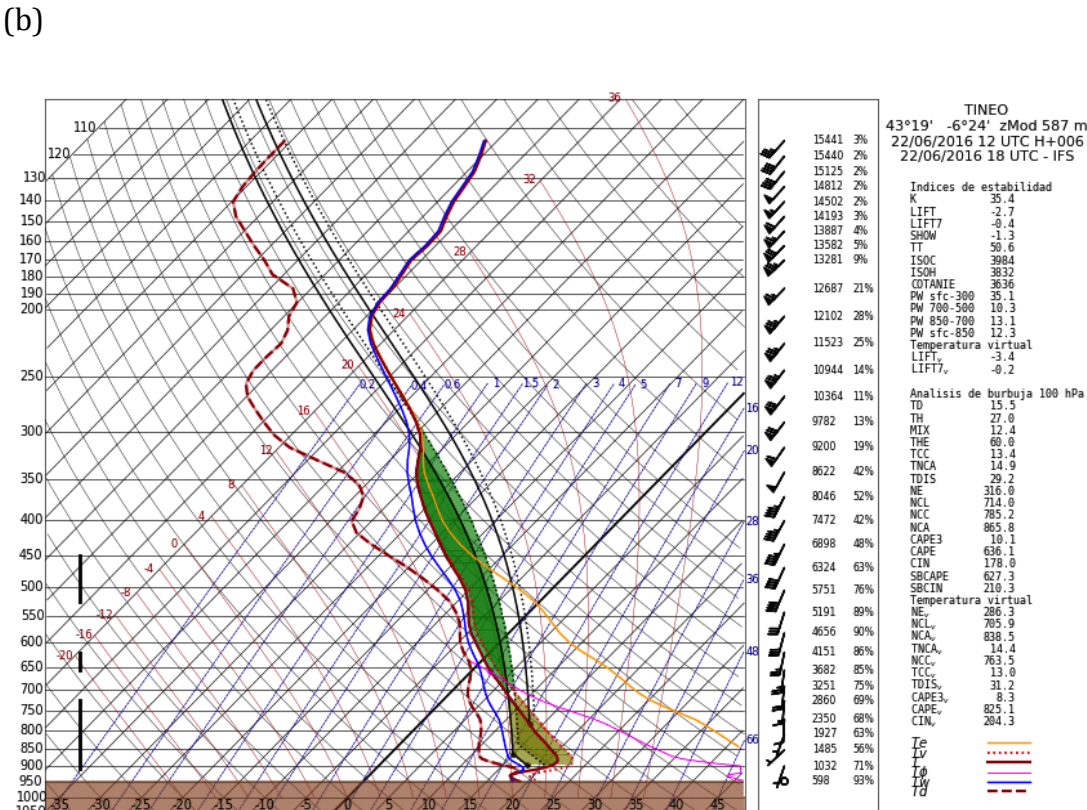
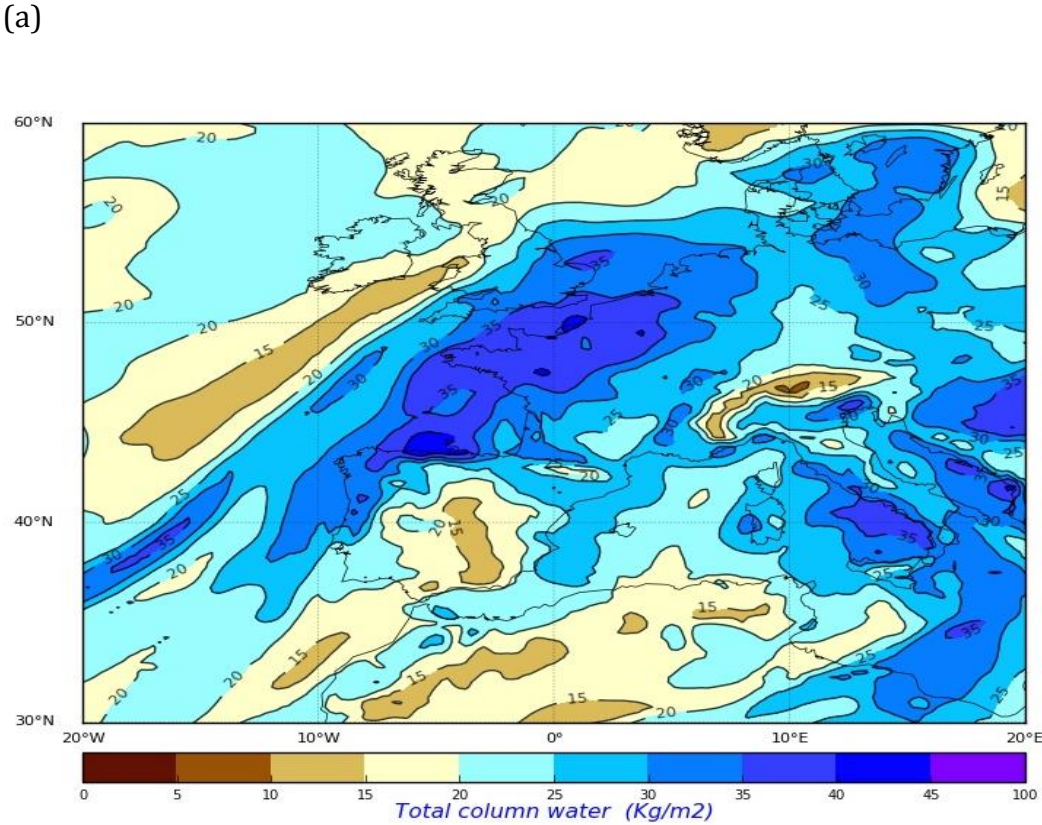
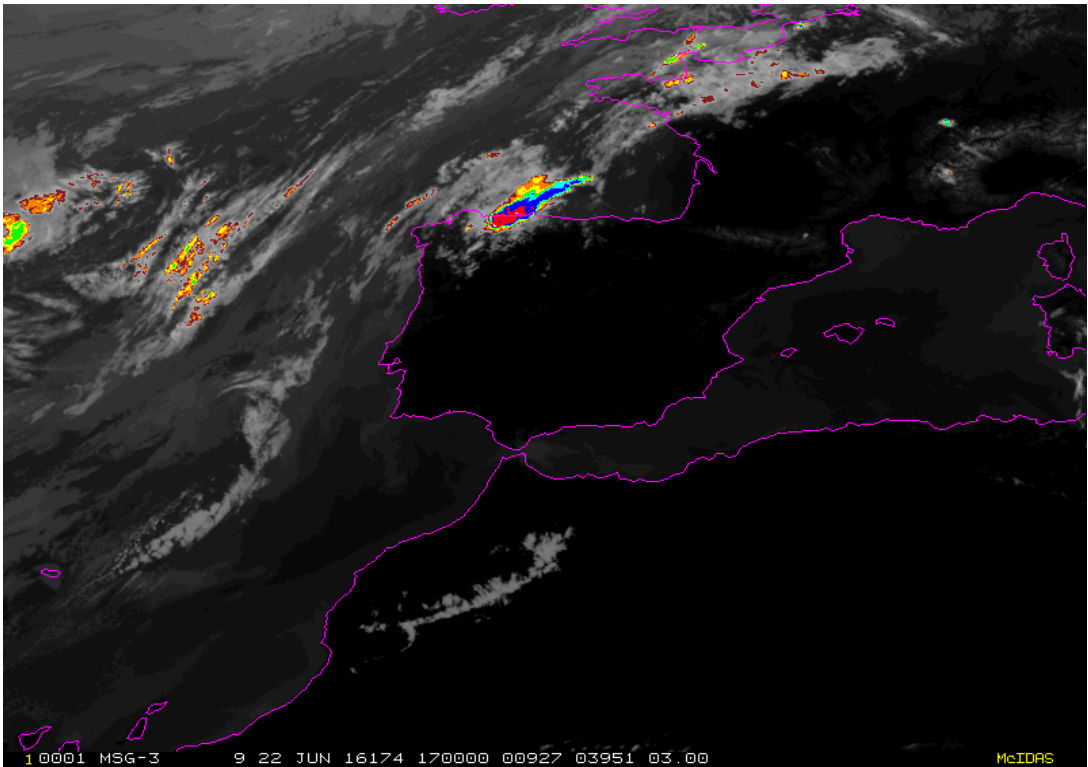


FIGURE 7

(a)



(b)

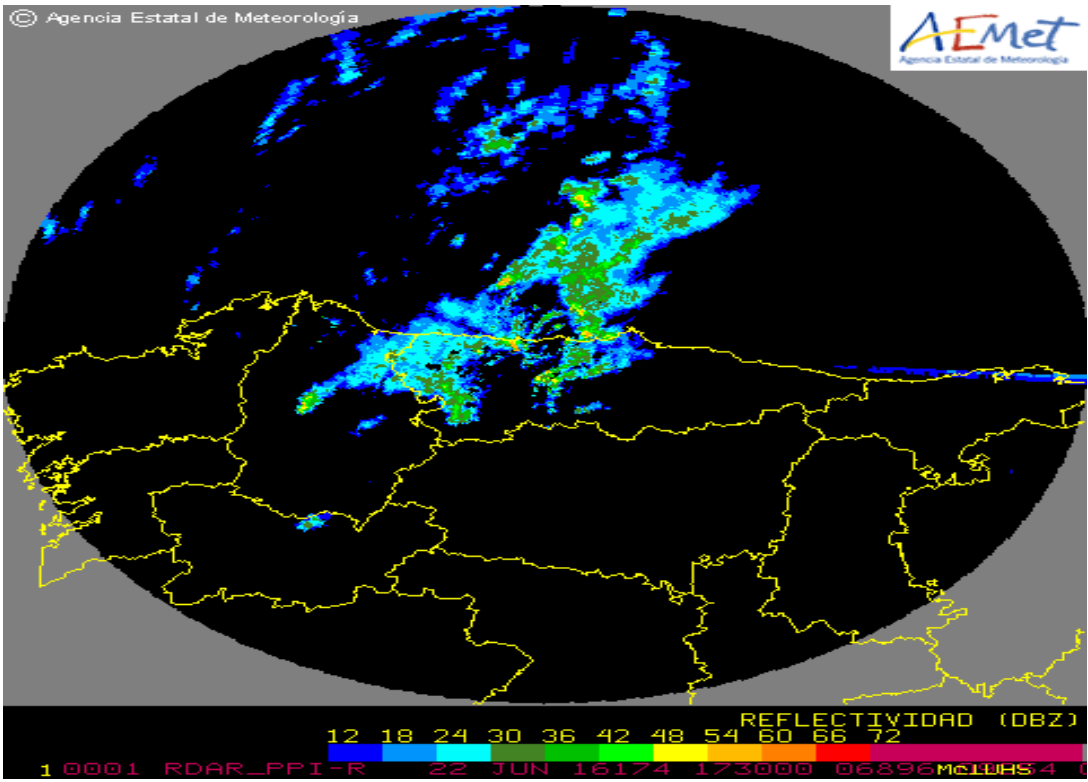


FIGURE 8

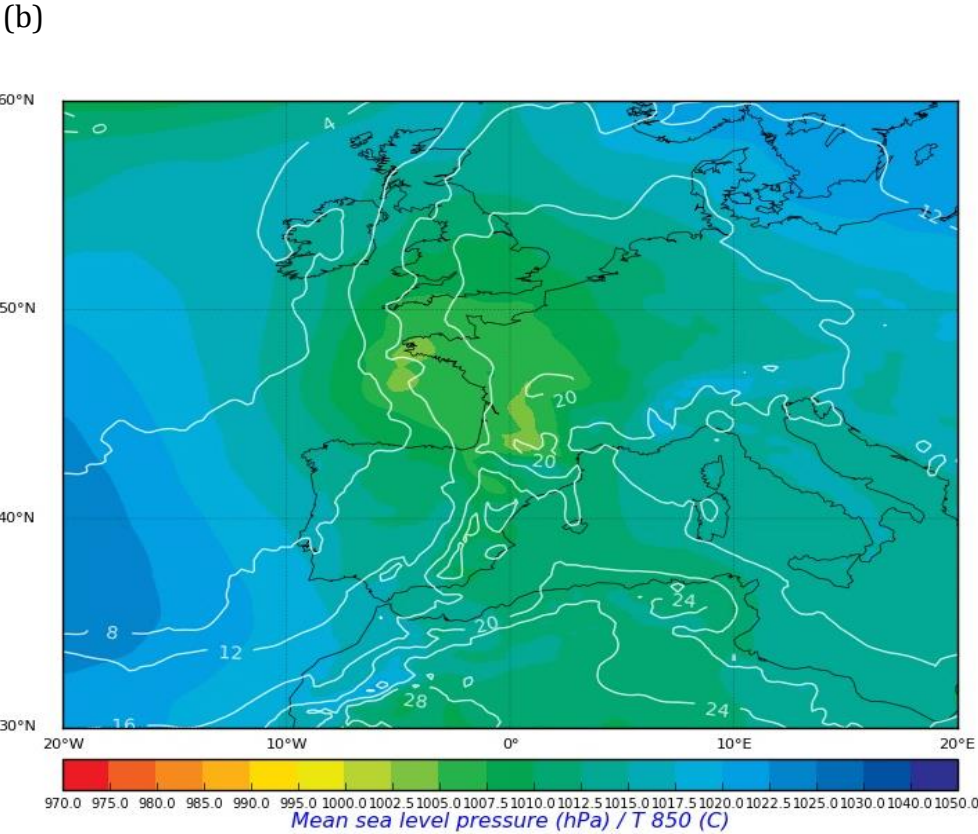
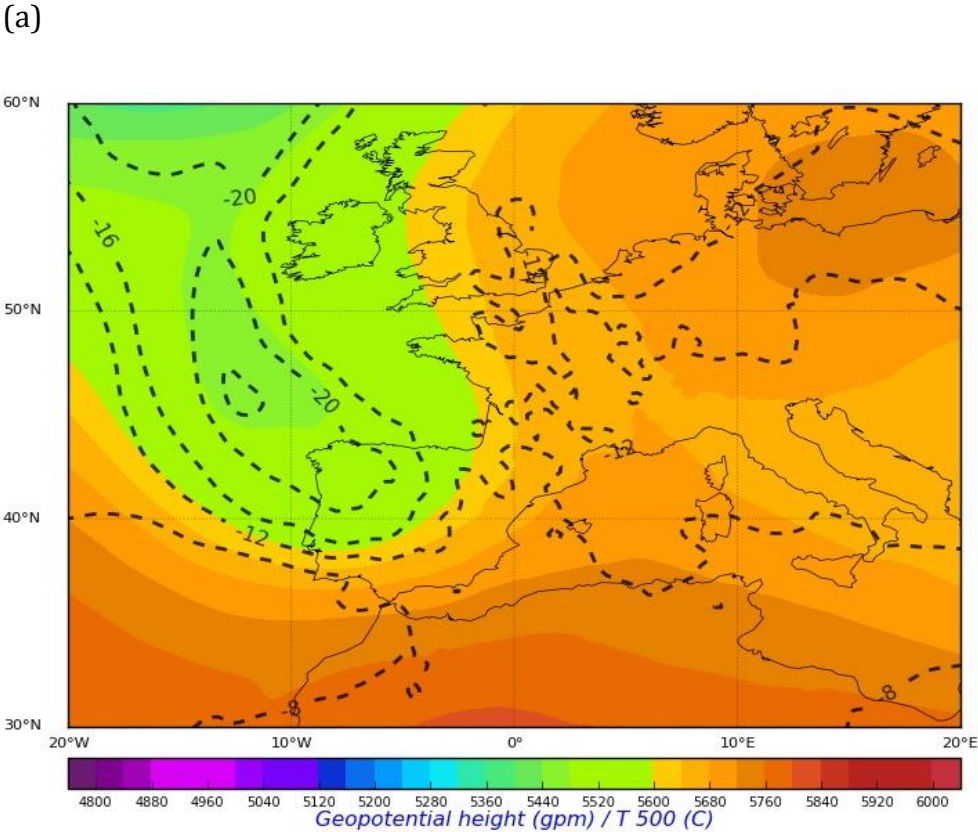
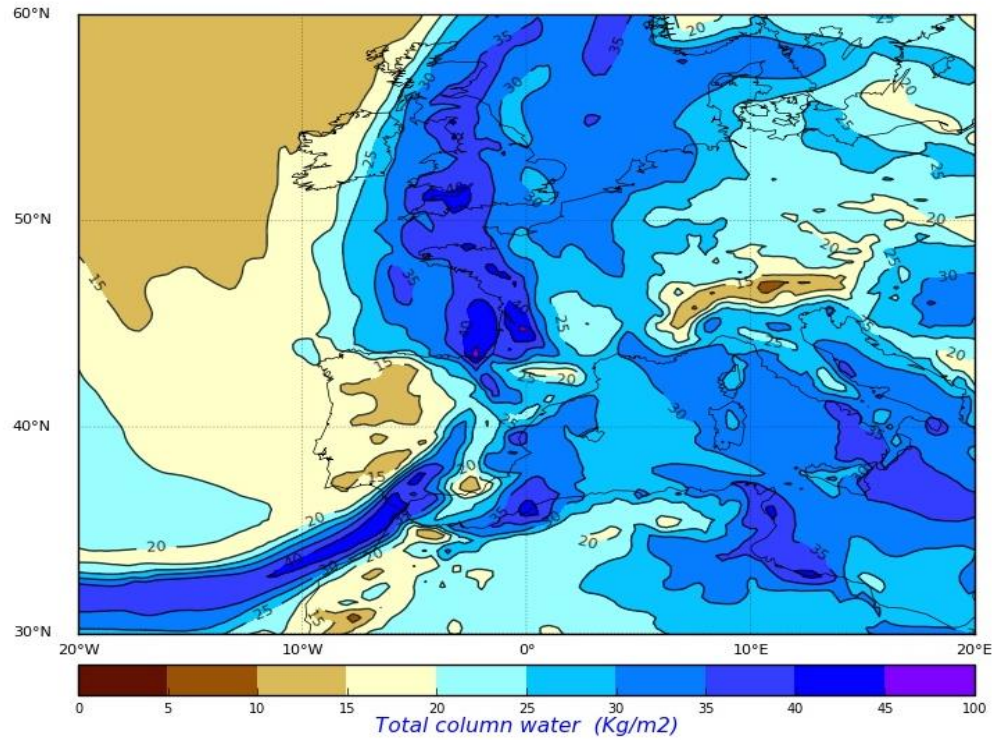


FIGURE 9

(a)



(b)

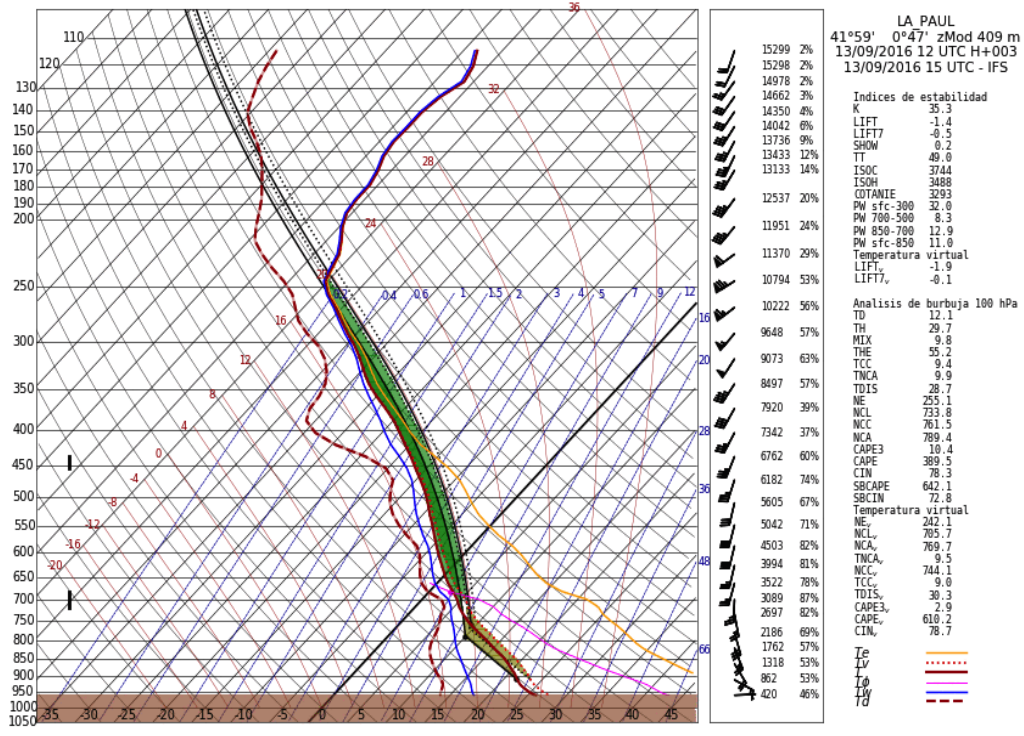


FIGURE 10

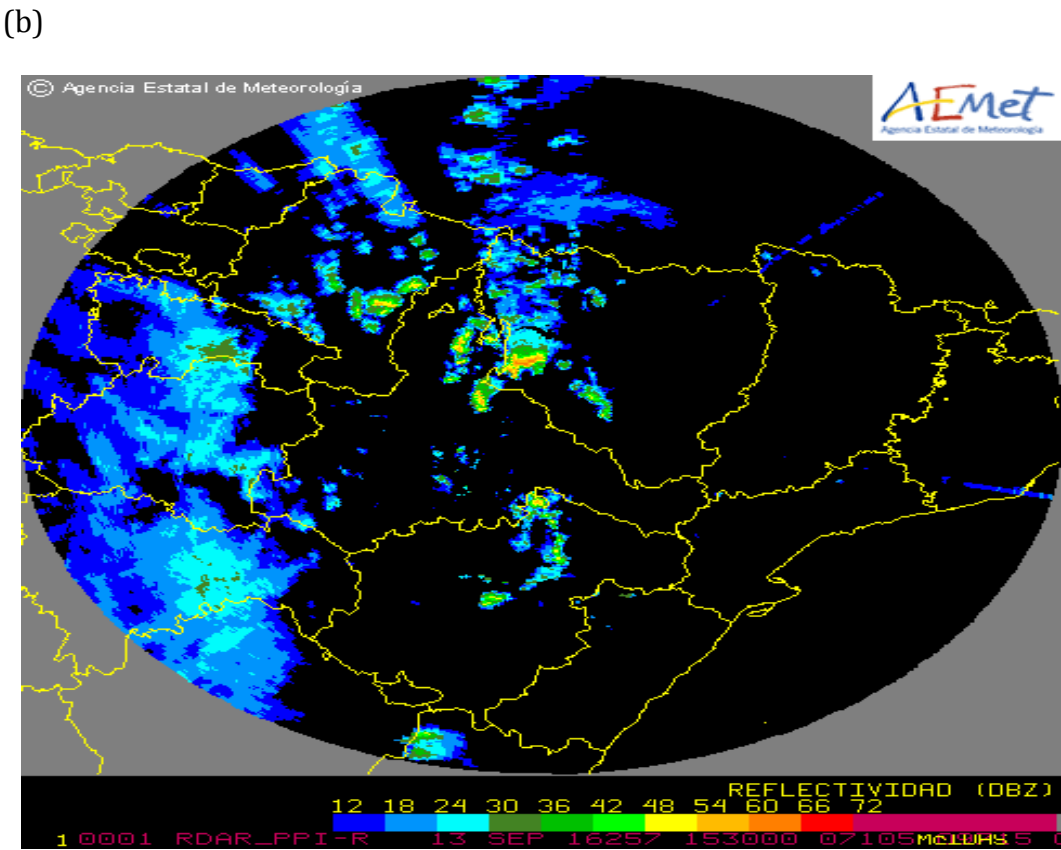
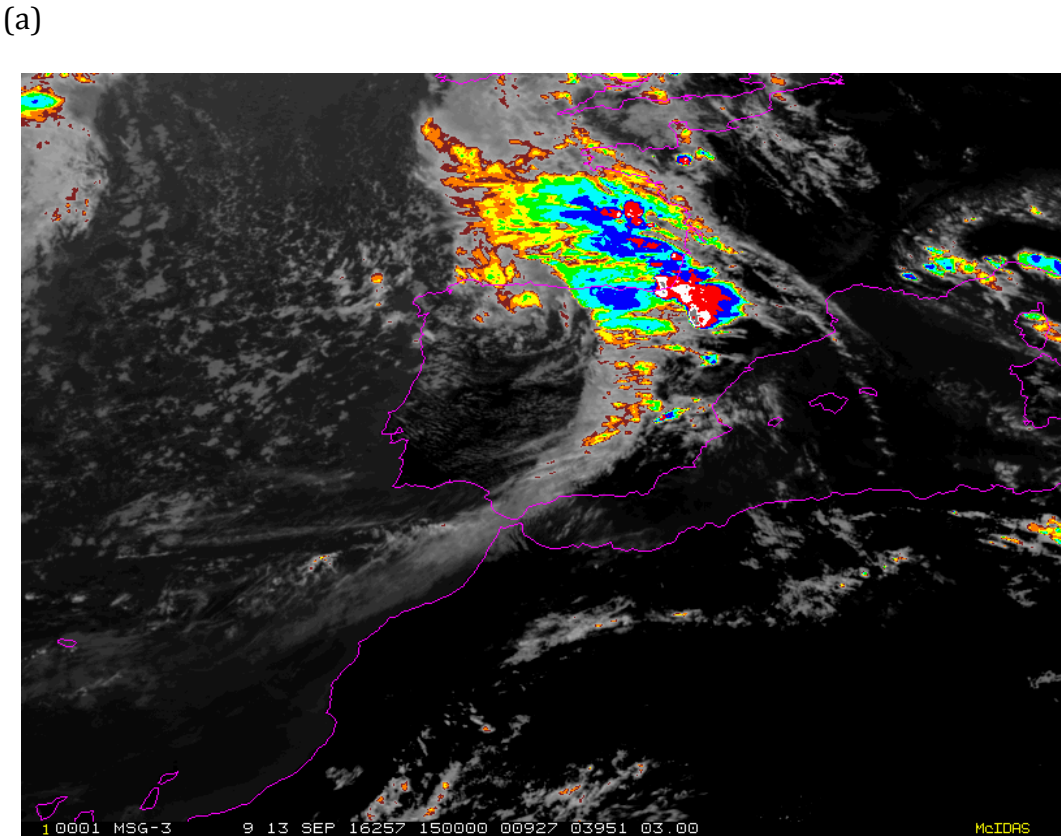


FIGURE 11

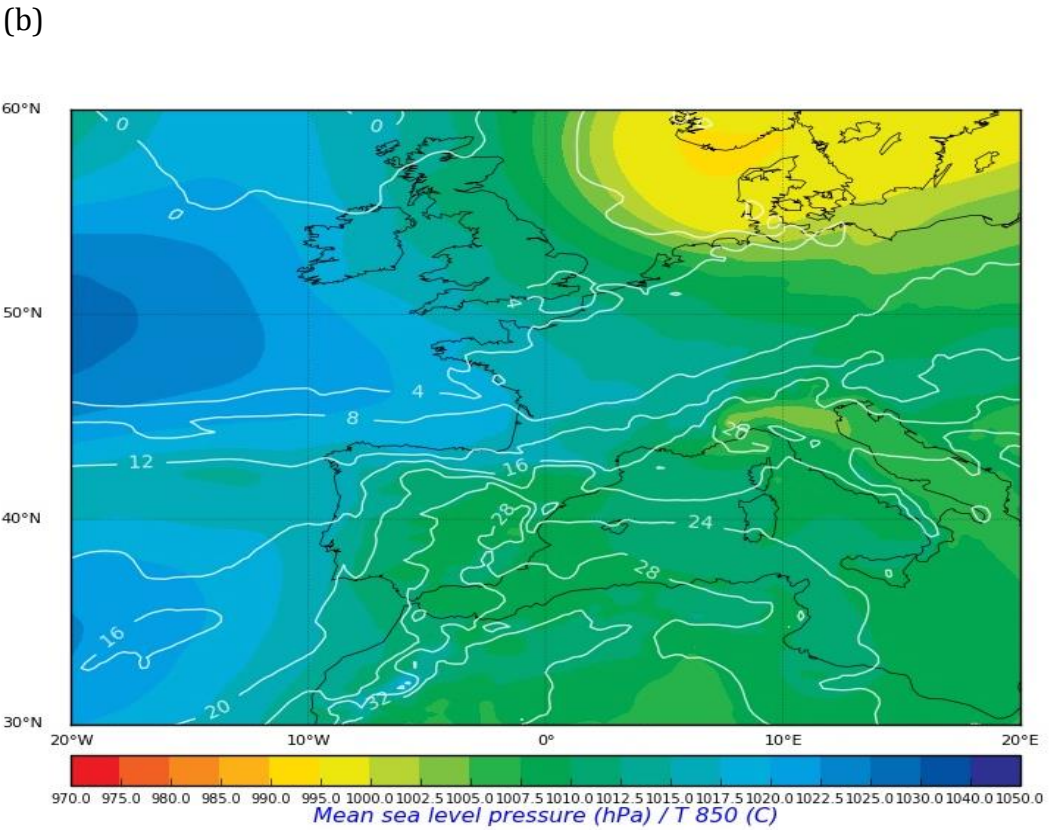
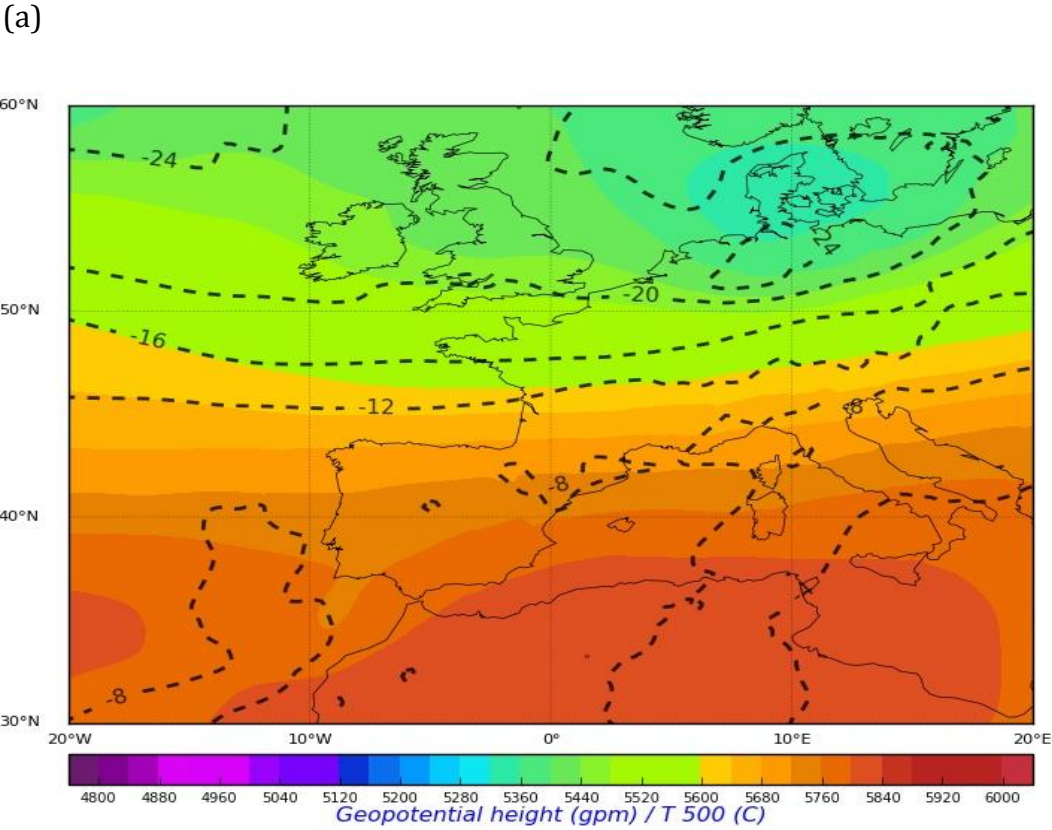
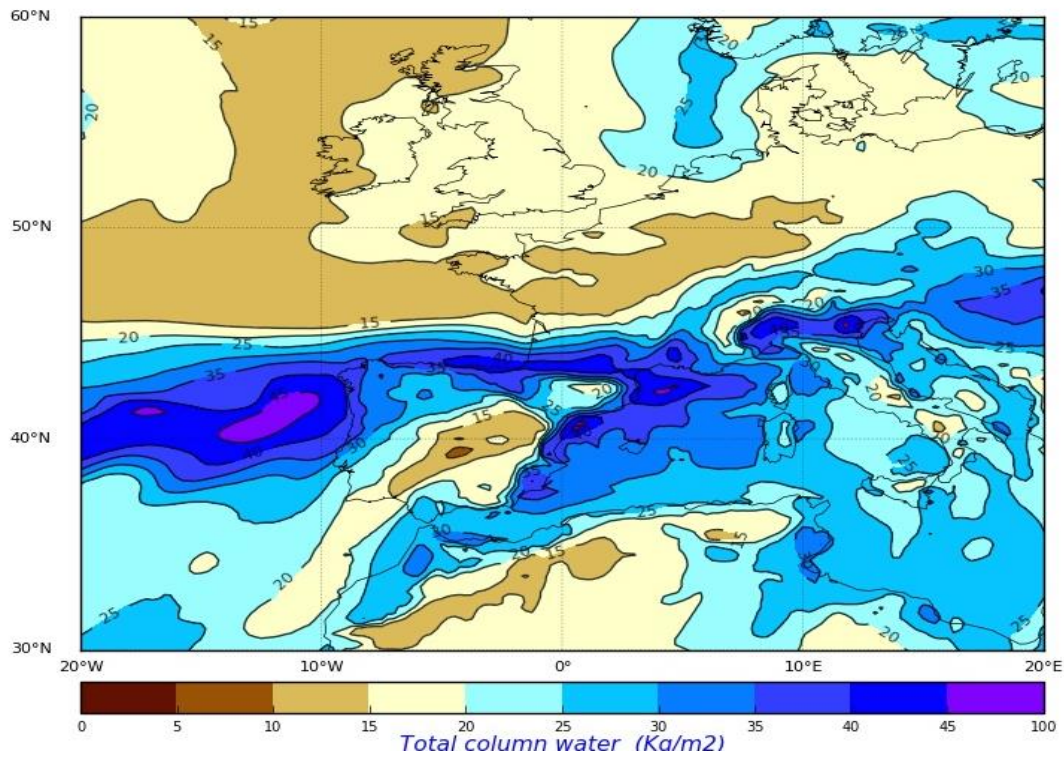


FIGURE 12

(a)



(b)

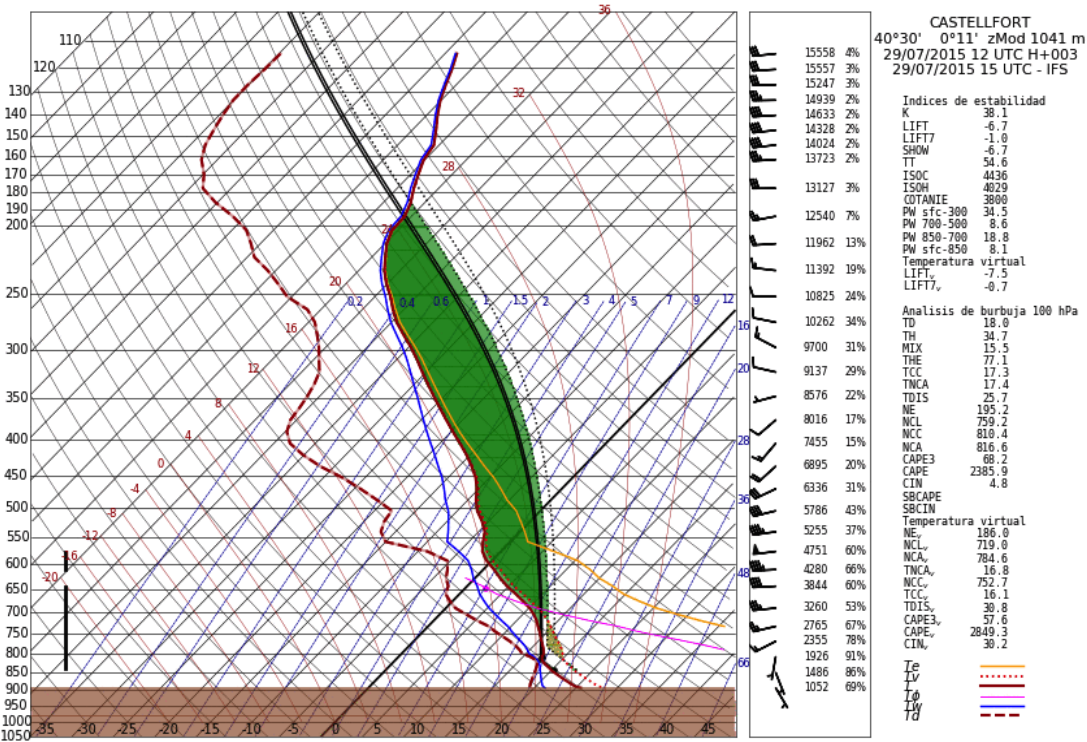
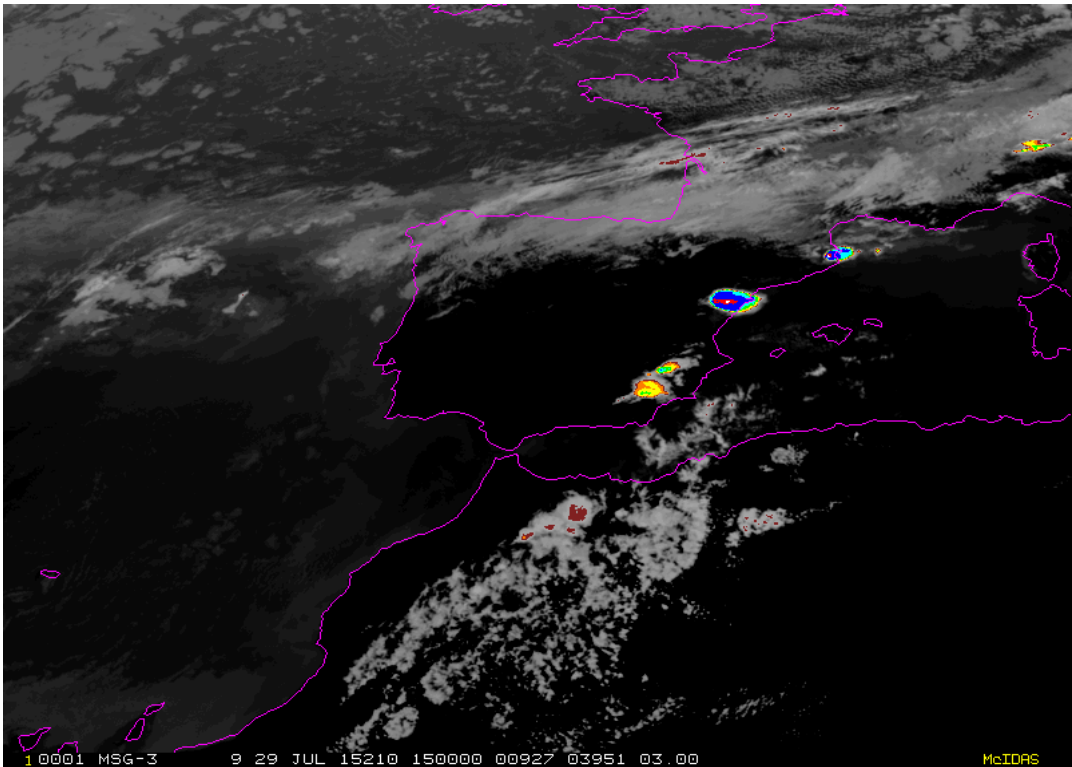
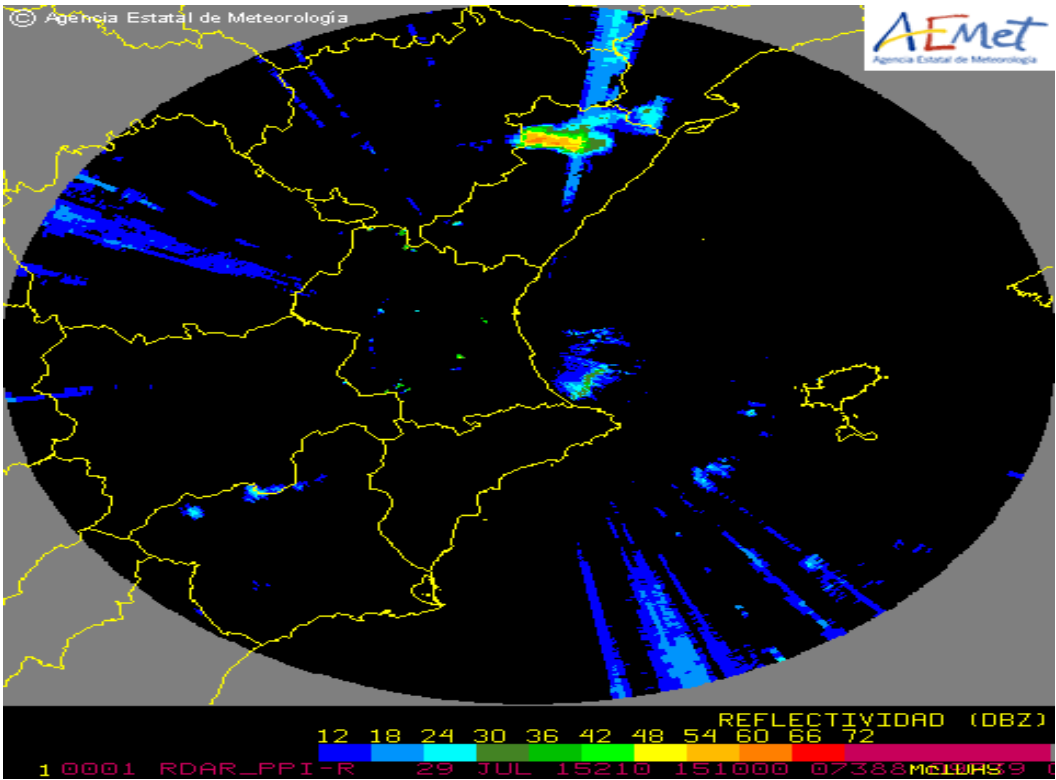


FIGURE 13

(a)



(b)



Declaration of interests

X The authors declare that they have no known competing financial interests or personal relationships that could have appeared to influence the work reported in this paper.

☐The authors declare the following financial interests/personal relationships which may be considered as potential competing interests: